Electronic changes induced by μ^+ in $PrIn_3$: Muon-spin-rotation observation and crystalline-electric-field model calculation

T. Tashma
Racah Institute of Physics, Hebrew University of Jerusalem, 91904 Jerusalem, Israel

A. Amato
Paul Scherrer Institute, CH-5232 Villigen PSI, Switzerland

A. Grayevsky
Racah Institute of Physics, Hebrew University of Jerusalem, 91904 Jerusalem, Israel

F. N. Gygax, M. Pinkpank, and A. Schenck
Institute for Particle Physics, ETH Zürich, CH-5232 Villigen PSI, Switzerland

N. Kaplan
Racah Institute of Physics, Hebrew University of Jerusalem, 91904 Jerusalem, Israel
(Received 15 May 1997)

Muon spin rotation in a single crystal of $PrIn_3$ reveals a significant influence of the implanted μ^+ on the local susceptibility χ_1 of the neighboring Pr^{+3} ions below ~ 60 K. It is found that χ_1 differs from χ_{bulk} both in magnitude and in symmetry. All of the changes are accounted for by a model calculation based on crystalline-electric-field theory. The extent of the μ^+-induced *magnetic changes* in the present system of $PrIn_3$ is rather modest compared to previously reported induced changes in $PrNi_5$. However, the model-derived *electronic-structure changes* around the μ^+ in $PrIn_3$ appear remarkably similar to those in $PrNi_5$, as is to be expected if the driving perturbation in both systems is primarily Coulombic in nature. [S0163-1829(97)03740-5]

I. INTRODUCTION

When studying condensed matter by the muon-spin-rotation (μSR) technique, the μ^+ probe may cause a local perturbation in its electronic environment, resulting in an inaccurate picture of the solid studied. In principle, this possibility applies to all μSR condensed-matter measurements. Such muon-induced effects were indeed detected recently in $PrNi_5$.[1] In the presence of the interstitial μ^+ in that system, the magnitude of the local susceptibility χ_1 along selected directions was shown to increase by up to an order of magnitude at temperatures below 20 K and the original bulk hexagonal anisotropy of χ was completely destroyed for χ_1. The reported susceptibility changes were assigned to local modifications in the crystalline electric field (CEF) acting on the Pr^{3+} ions next to the charged muon.

One should note that the μ^+ functions as a probe in materials only through its magnetic interaction with the surroundings. Consequently, magnetic changes in these same surroundings will inevitably lead to wrong conclusions concerning the material itself, as is evidenced by the $PrNi_5$ demonstration cited above. Thus, in addition to the basic scientific interest in the phenomena of muonic perturbations in solids, it is clearly of importance to assess the relevance of μ^+-induced effects when analyzing μSR data. Aiming for added insight into this problem, we started to look for similar effects in other magnetic systems. A rather simple reasoning dictated the $4f$ van Vleck paramagnets as candidates for the study. In such systems, the muon-induced effects occurring in the neighborhood of the μ^+ are expected to be especially pronounced because the magnetic properties of the singlet $4f$ configurations are sensitive even to minute changes in the local CEF. We chose to investigate the cubic PrM_3 series (M = In, Pb, Tl, Sn) for which the CEF level scheme is known to vary systematically (see Ref. 2). In this article we describe a μSR study performed on the first member of the series, a single-crystal $PrIn_3$.

The paper is organized as follows. A theoretical survey of the magnetic properties of $PrIn_3$ and the necessary μSR concepts are reviewed in Sec. II, followed by experimental details in Sec. III. The μSR results and a preliminary μ^+ site determination are presented in Sec. IV and the muon-induced local susceptibility is derived in Sec. V. The CEF model calculation and the associated perturbed electronic energy levels are described in Sec. VI. Finally, a semiquantitative comparison with the earlier $PrNi_5$ findings is included in Sec. VII. Preliminary results of the present study have been presented elsewhere.[3]

The magnetic properties of $PrIn_3$ have been described in detail in the past.[4] $PrIn_3$ belongs to the $Pm3m$ space group (Cu_3Au type), with Pr atoms at the cube corners of a fcc unit cell and In atoms occupying the face centers. Because of the cubic symmetry, the CEF Hamiltonian of the Pr ions must be of the form

$$\mathcal{H}_{\text{CEF}} = B_4^0 O_4^0 + 5B_4^0 O_4^4 + B_6^0 O_6^0 - 21B_6^0 O_6^4, \qquad (1)$$

where the value of the coefficients B_l^m is determined by the particular charge density around the Pr ion. Using the standard spherical coordinate system (R,Θ,Φ) with the Pr ion at the origin, the theoretical value of the B_l^m coefficients is determined by[5,6]

$$B_l^m \sim \int \frac{\rho(\mathbf{R}) Y_l^{m*}(\Theta,\Phi)}{R^{\lambda+1}} d\tau_R, \tag{2}$$

where the integration is carried out over all space. The crystal-field parameters for $PrIn_3$ are[2] $B_4^0 = -0.002\,52$ meV, and $B_6^0 = 0.000\,062$ meV. The energy eigenvalues derived by diagonalizing Eq. (1) with the above parameters are shown in Fig. 9 (left-hand side).

The two electrons in the unfilled $4f$ shells of the Pr ion form a $J=4$ multiplet, giving rise to a magnetic moment of $\mu_B g J$, with $g=0.8$. The In ions are nonmagnetic. In the presence of an external magnetic field, the Zeeman interaction splits the CEF energy levels, and for fields under ~ 10 T the magnetic susceptibility may be calculated by[7,5]

$$\chi_{\mathrm{CEF}} = \frac{\sum_n \left[\frac{(E_n^{(1)})^2}{kT} - 2E_n^{(2)} \right] \exp \frac{-E_n^{(0)}}{kT}}{\sum_n \exp \frac{-E_n^{(0)}}{kT}}, \tag{3}$$

with $E_n^{(0)}$ the unperturbed cubic CEF levels, $E_n^{(1)} = \mu_B g \langle \phi_n | J | \phi_n \rangle$, where ϕ_n are the unperturbed CEF wave functions, and

$$E_n^{(2)} = \sum_{n' \neq n} \mu_B^2 g^2 \frac{|\langle \phi_n | J | \phi_n' \rangle|^2}{E_n^{(0)} - E_{n'}^{(0)}}.$$

For magnetic singlet ϕ_n states, $E_n^{(1)} = 0$. Hence, in materials in which the CEF ground state is a singlet (as in $PrIn_3$), the low-temperature susceptibility is nearly temperature independent and depends reciprocally on the energy splittings of the excited levels above the ground state. Such materials are known also as van Vleck paramagnets.

In $PrIn_3$ one should take account also of a weak antiferromagnetic exchange coupling λ between the Pr ions. Within the mean-field approximation, we may use the expression for the exchange-enhanced susceptibility

$$\chi = \frac{\chi_{\mathrm{CEF}}}{1 - \lambda \chi_{\mathrm{CEF}}}. \tag{4}$$

Finally, we mention that in addition to the main contribution from the $4f$ electrons, there are two other minor sources of magnetic susceptibility, which we shall neglect hereinafter. The first is the Pauli paramagnetism χ_p of the conduction electrons, of the order of 10^{-3} emu/mole, i.e., an order of magnitude smaller than the $4f$ susceptibility. As will be evident later, we may safely ignore χ_p in the present context because it is temperature independent in our working temperature range. In addition, we shall ignore the diamagnetic susceptibility, which is of the order of 10^{-6} emu/mole and clearly negligible.

Relevant μSR concepts

The terminology adopted here will follow that of Refs. 1 and 8. With transverse field (TF) μSR, one measures basically the Larmor precession of the μ^+ spin under the influence of the magnetic field existing at the muon site inside the crystal lattice. The frequency of the precession is given by $\omega = \gamma_\mu B_\mu$, where γ_μ is the gyromagnetic ratio of the μ^+, $\gamma_\mu = 2\pi \times 13\,553.879\ \mathrm{s^{-1}\,G^{-1}}$ (± 0.2 ppm), and B_μ is the total magnetic field at the muon site. B_μ is a sum of both the external field and the various internal fields caused by the polarization of the material. Neglecting the diamagnetic and Pauli paramagnetic fields, the total field at the muon site is given by

$$\boldsymbol{B}_\mu = \boldsymbol{H} + \boldsymbol{B}_{\mathrm{hf},f}, \tag{5}$$

where $\boldsymbol{H}$ is the external field and $\boldsymbol{B}_{\mathrm{hf},f}$ is the hyperfine field originating from the polarization of localized $4f$ electrons in the Pr^{+3} ions. For simplicity, we include also the Lorentz and the demagnetization fields in $\boldsymbol{H}$.

The polarization of the $4f$ dipole moments affects the field at the muon site through two channels: directly, by creating a dipolar field at the muon site, and indirectly, by increasing the polarization of the conduction electrons thereby producing an additional contact field at the interstitial muon (e.g., the Ruderman-Kittel-Kasuya-Yosida mechanism). The field produced in both cases is proportional to the Pr^{+3} atomic magnetic moment μ_f,

$$\boldsymbol{B}_{\mathrm{hf},f} = \mathbf{A}_f \boldsymbol{\mu}_f = \mathbf{A}_f \boldsymbol{\chi}_f \boldsymbol{H}, \tag{6}$$

where $\mathbf{A}_f = A^{ij}$ is the effective hyperfine coupling tensor at the muon site and $\boldsymbol{\chi}_f = \chi^{ij}$ is the atomic susceptibility tensor. $\mathbf{A}_f$ decomposes accordingly into two parts: $\mathbf{A}_f = \mathbf{A}_{\mathrm{dip}} + \mathbf{A}_{\mathrm{con}}$. The dipolar part is a purely geometric tensor given by

$$A_{\mathrm{dip}}^{ij} = \sum_{4f \in \mathcal{L}} (1/r^3)(3x_i x_j / r^2 - \delta_{ij}), \tag{7}$$

where the summation extends over all the Pr^{3+} dipoles in the Lorentz sphere $\mathcal{L}$ and the vectors $\boldsymbol{r} = (x_1, x_2, x_3)$ point from the muon to each of the dipoles included in the summation. Equation (7) will be important in determining the muon site in Sec. IV C. $\mathbf{A}_{\mathrm{con}}$ does not have a simple expression, but if we reasonably assume that the coupling through the conduction electrons is isotropic in nature, then we can write $\mathbf{A}_{\mathrm{con}} = A_{\mathrm{con}} \mathbf{e}$, where $\mathbf{e} = \delta_{ij}$ is the unit tensor. If we further note that $\mathbf{A}_{\mathrm{dip}}$ is traceless, we obtain $\mathbf{A}_{\mathrm{con}} = \frac{1}{3}\mathrm{Tr}(\mathbf{A}_f)\mathbf{e}$.

It is convenient to define the relative frequency shift, or Knight shift,

$$K_\mu = \frac{|\boldsymbol{B}_\mu| - |\boldsymbol{H}|}{|\boldsymbol{H}|} = \frac{B_\mu}{H} - 1 = \frac{\omega}{\omega_0} - 1, \tag{8}$$

where $\omega_0 = \gamma_\mu H$. For the case of $\boldsymbol{B}_{\mathrm{hf},f}$ collinear with $\boldsymbol{H}$, we may use Eqs. (5) and (6) to derive the Knight shift originating from the $4f$ moments

$$K_f = |\mathbf{A}_f \boldsymbol{\chi}_f \boldsymbol{H}| / H. \tag{9}$$

If $B_{\mathrm{hf},f} \ll H$, as in the present case, we may relax the collinearity condition and consider for K_f just the projection of $\boldsymbol{B}_{\mathrm{hf},f}$ on $\boldsymbol{H}$, so that

$$K_f = \boldsymbol{h}\mathbf{A}_f\boldsymbol{\chi}_f\boldsymbol{h}, \tag{10}$$

where $\boldsymbol{h}=\boldsymbol{H}/|\boldsymbol{H}|$ is the unit vector along the external field. Note that if the external magnetic field is directed along one of the principle axes of the crystal, both Eqs. (9) and (10) reduce to the simple form

$$K_i = A^{ii}\chi_i . \tag{11}$$

The subscript f has been dropped for the sake of convenience. From Eq. (11) it is clear that a measurement of K_i supplemented by a knowledge of χ_i (or alternatively A^{ii}) will provide us a value for A^{ii} (or χ_i). This fact will be used in analyzing the temperature scans in Sec. IV B.

In cases where the magnetic field is not directed along one of the principle axes (as in the angular scan presented in Sec. IV A), one has to work with the general expression (10). Writing $\boldsymbol{h}$ in spherical coordinates, $\boldsymbol{h}=(\sin\theta\sin\varphi,\sin\theta\cos\varphi,\cos\theta)$, Eq. (10) turns into[1]

$$\begin{aligned} K_f(\theta,\varphi) = {} & \frac{1}{3}(A^{xx}\chi_x + A^{yy}\chi_y + A^{zz}\chi_z) \\ & + \frac{2}{3}\left(A^{zz}\chi_z - \frac{1}{2}(A^{xx}\chi_x + A^{yy}\chi_y)\right)P_2^0(\cos\theta) \\ & + \frac{1}{3}A^{xz}(\chi_x+\chi_z)P_2^1(\cos\theta)\cos\varphi \\ & + \frac{1}{3}A^{yz}(\chi_y+\chi_z)P_2^1(\cos\theta)\sin\varphi \\ & + \frac{1}{6}(A^{xx}\chi_x - A^{yy}\chi_y) \\ & \times P_2^2(\cos\theta)\cos 2\varphi + \frac{1}{6}A^{xy}(\chi_x+\chi_y) \\ & \times P_2^2(\cos\theta)\sin 2\varphi . \end{aligned} \tag{12}$$

In the special case of fourfold symmetry around the z axis, which will be found relevant to our system, we have (i) $A^{xx}=A^{yy}$, (ii) $\chi_x=\chi_y$, and (iii) $A^{xy}_{\rm dip}=A^{xz}_{\rm dip}=A^{yz}_{\rm dip}=0$, leading to $A^{xy}=A^{xz}=A^{yz}=0$ (as $\mathbf{A}_{\rm con}$ is diagonal). The third statement is verified by noting that with axial symmetry, for each Pr dipole at a point (x,y,z), there is one at $(-x,y,z)$. Summing expression (7) for $A^{ij}_{\rm dip}$ by adding each time the joint contribution of such pairs, we find immediately that both $A^{xy}_{\rm dip}$ and $A^{xz}_{\rm dip}$ vanish. A similar reasoning leads to the vanishing of the third mixed element $A^{yz}_{\rm dip}$. With these three special conditions, the general expression (12) reduces to

$$\begin{aligned} K_f(\theta) = {} & \frac{1}{3}(2A^{xx}\chi_x + A^{zz}\chi_z) + \frac{2}{3}(2A^{zz}\chi_z - A^{xx}\chi_x) \\ & \times P_2^0(\cos\theta). \end{aligned} \tag{13}$$

II. EXPERIMENT

The single crystal of $PrIn_3$ was grown and characterized as described earlier.[3] A cylindrical sample was shaped by spark erosion, with the cylinder axis parallel to the crystallographic [110] axis. The same crystal sample was used for the susceptibility measurement and for the TF μSR data presented here. The susceptibility χ was measured by a commercial squid magnetometer (Quantum Design) between 5 K and room temperature. The results are shown in Fig. 1 and are in good agreement with previously published data,[4] except for a small rise at temperatures below 4 K, which seems absent from the previous data. (Note, however, that the accuracy of the older data does not enable one to ascertain the absence of a similar rise there.) A possible explanation of the small rise is given elsewhere.[9]

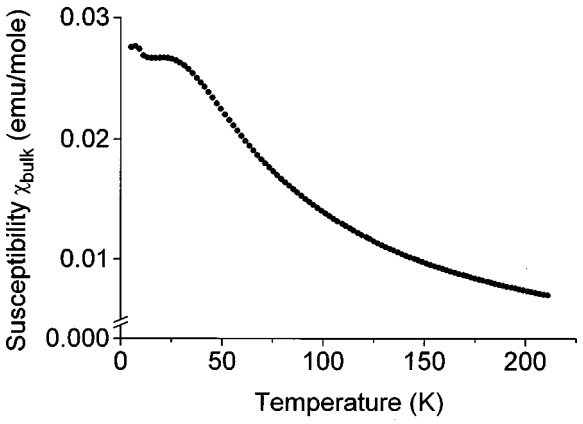

FIG. 1. Bulk susceptibility of $PrIn_3$.

The TF μSR measurements were performed using the πM3 and μE1 beam lines in an external magnetic field of $H=6$ kOe. The field direction in the crystal could be rotated in a plane perpendicular to the [110] cylinder axis. The external field value was measured with a NMR probe and a background signal from the copper sample holder served as a convenient continuous *in situ* field monitor. The temperature was varied in the range $3.3\ \mathrm{K}\leqslant T\leqslant 100\ \mathrm{K}$.

III. RESULTS

In this section we present the Knight shift results. We begin by describing results of an angular scan at constant temperature, which revealed the type of site occupied by the muon in the $PrIn_3$ unit cell. Next we will show results of temperature scans, which point to local changes in the bulk susceptibility around muons in $PrIn_3$. In addition, by analyzing just the higher-temperature data, a single muon site is determined.

A. Angular scan and an evaluation of the muon site

The TF μSR signal in $PrIn_3$ revealed in general three distinct frequencies.[3] A typical frequency domain spectrum is shown in Fig. 2. The intensity ratio of the signals labeled $F1$ and $F2$ is given by $I(F1):I(F2)=2:1$. The angular de-

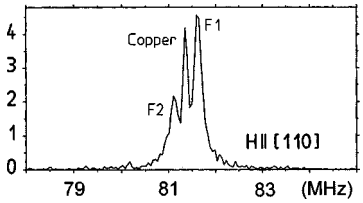

FIG. 2. Typical μSR signal spectrum in $PrIn_3$ at 15 K. The intensity ratio of the signals, $F1:F2=2:1$, is clearly depicted.

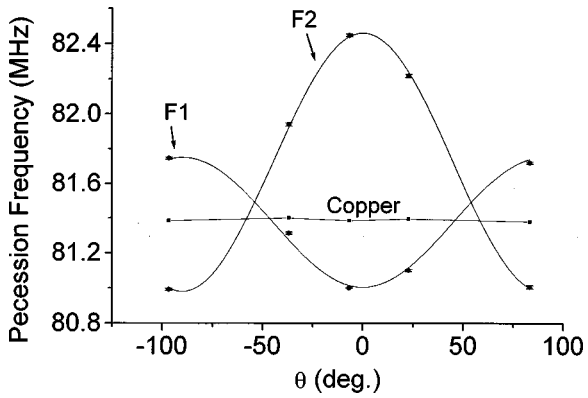

FIG. 3. Angular dependence of the μ^+ precession frequencies. The external field was rotated in the {1,1,0} plane and θ indicates the angle between the external field and the crystallographic [0,0,1] axis. The two sets of frequencies, labeled $F1$ and $F2$, indicate two magnetically nonequivalent muon sites.

pendence of the different μSR signal frequencies, obtained at 15 K by rotating the external field in the {1,1,0} plane, is shown as points in Fig. 3. The observed shifts from the vacuum frequency of 81.4 MHz are caused mainly by the dipolar field existing at the muon site, as detailed in Sec. II B. Along the horizontal axis, θ denotes the angle between the field direction and the crystallographic [001] axis. (See Fig. 4, where θ is drawn on the shaded {1,1,0} plane of rotation.) The constant frequency signal seen at approximately 81.4 MHz is due to the copper sample holder and will be of no interest except as a reference.

The solid curves in Fig. 3 represent best fits of ''theory'' functions to the two observed frequency signals $F1$ and $F2$. Specifically, we find

$$F1(\theta)\ \ (\mathrm{MHz}) = 81.50 - 0.50 P_2^0(\cos\,\theta), \tag{14}$$

$$F2(\theta)\ \ (\mathrm{MHz}) = 81.47 + 0.98 P_2^0(\cos\,\theta).$$

The fits (14) follow the general form (12) expected of a field created by a system of dipoles. Notice the $-\frac{1}{2}$ ratio between the coefficients of $P_2^0(\cos\,\theta)$ in $F1$ and $F2$, to which we will return later.

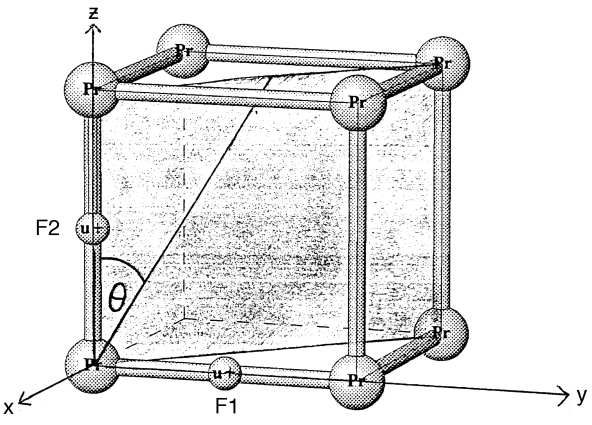

FIG. 4. Two equivalent sites of the μ^+ inside the crystal lattice, marked by $F1$ and $F2$ as in Fig. 3. The shaded {1,1,0} plane is the rotation plane of the external field and the angle θ within it composes the x axis of Fig. 3.

We can now try to identify the muon site. The coordinate system drawn in Fig. 4 will be adopted hereinafter. We start by noticing that the two signals $F1$ and $F2$ coincide for **H** along the [111] direction. This proves the two signals originate from crystallographically *equivalent* sites, with a site multiplicity of 2 or higher. In addition, we will now show that the muon producing the $F2$ signal is situated at a position with fourfold z-axis symmetry and the one producing $F1$ at a site with fourfold y- (or x-) axis symmetry. In the theoretical survey it was found that the general angular dependence (10) reduces to the form (13) in the special case of fourfold z-axis symmetry. However, the $F2$ fit in Eq. (14) is identical in form to Eq. (13), pointing to a site of z-axis symmetry. Next let us look at $F1$. Because $F1$ is crystallographically equivalent to $F2$, it should be obtainable from $F2$ by interchanging z with either y or x. Choosing y, we would expect the symmetry around $F1$ to be *identical* to that around $F2$, but *transferred* from the z to the y axis. Thus the theoretical angular dependence for $F1$ is derived in the same manner as for $F2$, giving

$$[K_f(\theta)]_{F1} = \frac{1}{3}(2A_{F1}^{xx}\chi_x + A_{F1}^{yy}\chi_y) - \frac{1}{2} \times \frac{2}{3}(2A_{F1}^{yy}\chi_y - A_{F1}^{xx}\chi_x)P_2^0(\cos\,\theta) + \frac{1}{6}(A_{F1}^{xx}\chi_x - A_{F1}^{yy}\chi_y)P_2^2(\cos\,\theta)\cos 2\varphi. \tag{15}$$

Notice that the subscript $F1$ was assigned to all elements of **A** in Eq. (15), in order to emphasize that they should be calculated with respect to the muon located at site 1, in contrast to expression (13), which is relevant *only* to muon at site 2 (z-axis symmetry).

Now, when comparing expressions (13) and (15), it becomes clear that, taking into account that (i) A_{F1}^{yy} in Eq. (15) is identical to A_{F2}^{zz} in Eq. (13), (ii) A^{xx} is identical for both sites, and (iii) for the {1,1,0} plane, $\cos 2\varphi = 0$, it follows that the pair of theoretical expressions (13) and (15) is similar in form to the pair of experimental fits (14), *including* the $-\frac{1}{2}$ ratio for the coefficients, mentioned earlier. Thus we have proved that the muons are located at sites of fourfold axial symmetry. A list of all the possible interstitial sites in the $Pm3m$ structure may be found, e.g., in Ref. 13. Of these, $1a$, $1b$, $3c$, $3d$, $6e$, $6f$, and $8g$ have the necessary fourfold axial symmetry. However, $1a$ and $3c$ are already occupied by Pr or In atoms and $1b$,$8g$ will inevitably produce just one signal in the presence of a magnetic field. Hence we are left with just two possible sites: $6e$, of the type $(0,0,d)$, and $6f$, of the type $(0.5,0.5,d)$. Note that (0,0,0.5) is the $3d$ site.

As will be shown in Sec. III C, the $6f$ site must be ruled out and the correct muon site for $F2$ is (0,0,0.5) [or, equivalently, (0,0.5,0) for $F1$]. The situation is illustrated in Fig. 4. It is clear that under the influence of a magnetic field rotating in the {1,1,0} plane, the equivalent $6e$ sites will delineate into two magnetically inequivalent locations, demonstrated in the figure by $F1$ and $F2$. The shifts of the two signals differ as a result of the different dipolar fields. We also see that the number of $F1$ sites is indeed double that of $F2$ sites, accounting for the observer 2:1 signal intensity ratio mentioned earlier.

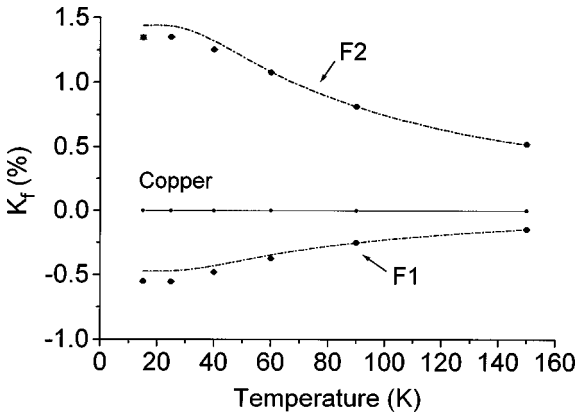

FIG. 5. Knight shift as a function of temperature, in an external field parallel to the [001] axis. The points are the experimentally measured values. The dashed lines are theoretical values, calculated assuming a constant linear scaling between the Knight shift and the $PrIn_3$ bulk susceptibility (see the text for details).

B. Temperature scan

In this section we present the main results of the paper. The Knight shifts of $F1$ and $F2$ were measured as a function of temperature, in a constant external field of 6006 Oe directed parallel to the principal [001] axis. The results are shown as points in Fig. 5. All data are corrected for bulk demagnetization and Lorentz fields in a manner similar to that detailed in Ref. 1. Note that the [001], [010], and [100] directions remain the principle axes of the system in the presence of a muon either at site $F1$ or at site $F2$ (see Fig. 4). Therefore, we expect the Knight shifts measured with the field along the [001] direction to follow the linear relation (11) with $i=z$. However, if we look at Fig. 6, where the Knight shift data from Fig. 5 is plotted against the bulk susceptibility of $PrIn_3$, with the temperature as an implicit parameter, we see definite deviations from the expected linearity. These deviations point to a possible muon-induced change in the local susceptibility, as will be discussed in detail further on. Only temperatures above 15 K were considered in order to avoid uncertainties arising from the unexpected rise in the bulk susceptibility seen in Fig. 1.

As is clear from Fig. 6, we chose to assume that the high-temperature region is the linear region. This assumption was shown to be justified in similar, earlier, graphs obtained with $PrNi_5$.[1] Moreover, it is strongly supported by theoretical considerations presented in Sec. VI.

It is possible to infer the same deviation of K from $\chi_{\rm bulk}$ in another way. Suppose we *do* assume that the high-temperature linear scaling between K and $\chi_{\rm bulk}$ in Fig. 5 is kept at all temperatures. Then let us ''force'' the same scaling to hold also at low temperatures and use it to compute K out of the values of $\chi_{\rm bulk}$. These artificially ''correct'' values of K are given by the dashed lines in Fig. 5. Again we see that the predicted and measured values of K do not agree.

From the high-temperature region in Fig. 6 we can derive the value of A_f^{zz}, by using Eq. (11) with $i=z$. We find $A_f^{zz}(F1)=-0.19\pm0.01$ mole/emu and $A_f^{zz}(F2)=0.54\pm0.02$ mole/emu. The error boundaries in $\mathbf{A}_f$ include the experimental uncertainties in K and $\chi_{\rm bulk}$ and also an estimate of the error involved in assuming that the high-temperature region is linear. Because of the specific geometric arrangement of the muons labeled $F1$ and $F2$ it is possible now to write the complete experimental $\mathbf{A}_f$ tensor

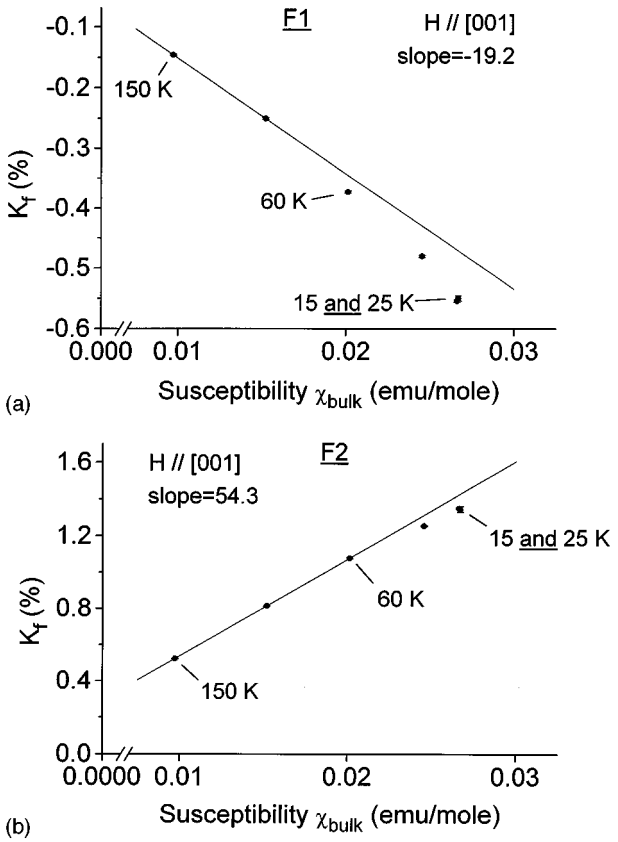

FIG. 6. (a) and (b) are the Knight shift of signals $F1$ and $F2$, respectively, against the $PrIn_3$ bulk susceptibility. The temperature is an implicit parameter. The straight lines are linear regressions to the high-temperature regions.

$$\mathbf{A}_f(F1)=\begin{pmatrix}-0.19 & 0 & 0\\ 0 & 0.54 & 0\\ 0 & 0 & -0.19\end{pmatrix}\frac{\text{mole}}{\text{emu}},$$

$$\mathbf{A}_f(F2)=\begin{pmatrix}-0.19 & 0 & 0\\ 0 & -0.19 & 0\\ 0 & 0 & 0.54\end{pmatrix}\frac{\text{mole}}{\text{emu}}.$$

The nondiagonal elements were shown to vanish theoretically in Sec. II B. Following the definitions presented in Sec. III, we may now decompose $\mathbf{A}_f$ into its two independent parts $\mathbf{A}_{\rm con}=(0.05\pm0.015)\mathbf{e}$ mole/emu, representing the contact coupling, and

$$\mathbf{A}_{\rm dip}(F2)=\begin{pmatrix}-0.24 & 0 & 0\\ 0 & -0.24 & 0\\ 0 & 0 & 0.49\end{pmatrix}\frac{\text{mole}}{\text{emu}}, \qquad (16)$$

representing the direct dipolar field coupling. A completely analogous expression applies of course to $\mathbf{A}_{\rm dip}(F1)$.

C. Verification of the μ^+ site

It is now possible to verify the suggested $(0,0,d=0.5)$ stopping site. First we would want to exclude the possibility of a $6f$ site of the type $(0.5,0.5,d)$. By performing an independent dipolar sum calculation based solely on expression (7), taking the muon site within the unit cell to be $(0.5,0.5,d)$ (an $F2$ site), we obtained for different d values $A^{zz}_{\mathrm{dip,calc}}(d=0.5)=0$ mole/emu, $A^{zz}_{\mathrm{dip,calc}}(d=0.3)=-0.04$ mole/emu, $A^{zz}_{\mathrm{dip,calc}}(d=0.1)=-0.126$ mole/emu, and $A^{zz}_{\mathrm{dip,calc}}(d=0.0)=-0.14$ mole/emu. A comparison of these results with the experimental value in Eq. (16) eliminates the possibility of a $(0.5,0.5,d)$ site. Note that the values $d=0$ and $d=0.5$ are brought merely as limiting cases, not possible in themselves.

We now performed the same calculation for different $(0,0,d)$ sites. For the (0,0,0.5) trial we obtained

$$\mathbf{A}^{\mathrm{calc}}_{\mathrm{dip}}(F2)=\begin{pmatrix} -0.245 & 0 & 0 \\ 0 & -0.245 & 0 \\ 0 & 0 & 0.491 \end{pmatrix}\frac{\mathrm{mole}}{\mathrm{emu}}.$$

Here the results are very close to the experimentally derived values, indicating that the muon is indeed located at (0,0,0.5). Considering the error boundaries of the experimental $\mathbf{A}_{\mathrm{dip}}$ in Sec. III B, we conclude that $d=0.5\pm0.04$. We are now in a position to investigate the observed low-temperature deviations of the Knight shift from linearity with χ_{bulk}.

IV. LOCAL SUSCEPTIBILITY

Figure 6 shows that at low temperatures the muon Knight shift in $PrIn_3$ deviates from the expected linear scaling with the bulk susceptibility. The conclusion must be that the μ^+ is monitoring a different susceptibility than the original bulk one, caused locally by its own presence in the crystal. Hence, as a next step, we will use the Knight shift data in Fig. 6 to find the new local Pr^{+3} susceptibility affecting the muon. To keep things simple, we will make the following assumptions. (i) The muon does not change the original $PrIn_3$ lattice constant. (ii) Only the susceptibility of the two nearest Pr^{+3} ions is affected by muon. (iii) Only the two nearest Pr^{+3} ions contribute to the contact interaction at the muon site. These assumptions are similar to those in Ref. 1 and are justified by the same reasoning. The third assumption, concerning the contact interaction, will be discussed in more detail later on. The last two assumptions allow us to decompose the hyperfine field at the muon site into a contribution from the nearest Pr neighbors and a contribution from all the rest of the Pr ions in the Lorentz sphere.

Let us designate by χ_i^{local} the new altered susceptibility of the two nearest Pr ions, while the original Pr susceptibility will be called χ^{bulk}. Based on the assumptions just made, the theoretical expression (11) for the Knight shift of $F2$ with the external field in the z direction [to fit the data in Fig. 6(b)] may be written as

$$K(F2)=(A^{zz}_{\mathrm{dip,NN}}+A_{\mathrm{con}})\chi_z^{\mathrm{local}}+A^{zz}_{\mathrm{dip,(1-NN)}}\chi^{\mathrm{bulk}}. \quad (17)$$

The subscript NN is used to signify that the sum in A_{NN} should include only the two nearest Pr neighbors, whereas the subscript $1-\mathrm{NN}$ indicates summation on all *other* Pr ions in the Lorentz sphere. In order to write a similar expression for $F1$, note that because the two sites are crystallographically equivalent, it is possible to consider the two signals as if originating from a *single* muon site, while the external field changes direction. For a μ^+ situated at (0,0,0.5), an external field along the the z axis produces $F2$ and an external field along the x axis will produce $F1$. With this transformation, one finds

$$K(F1)=(A^{yy}_{\mathrm{dip,NN}}+A_{\mathrm{con}})\chi_y^{\mathrm{local}}+A^{yy}_{\mathrm{dip,(1-NN)}}\chi^{\mathrm{bulk}}. \quad (18)$$

We can now isolate and compute the values of χ_z^{local} and χ_y^{local} in Eqs. (17) and (18) by substituting known or readily available values for the other variables. Values for $K(F2)$ and $K(F1)$ are available in Fig. 6, χ^{bulk} data are given in Fig. 1, and the value $A_{\mathrm{con}}=0.05$ mole/emu was already determined in Sec. IV B. Finally, by summing only on nearest neighbors in expression (7), we obtain the values $A^{zz}_{\mathrm{dip,NN}}=0.463$ mole/emu and $A^{yy}_{\mathrm{dip,NN}}=-0.23$ mole/emu, from which we compute the values of $A^{zz}_{\mathrm{dip,(1-NN)}}$ and $A^{yy}_{\mathrm{dip,(1-NN)}}$ using the total $\mathbf{A}_{\mathrm{dip}}$ that was already determined in Sec. IV B. The resulting values of $\chi^{\mathrm{local}}_{z,y}$ vs T are shown as points with the associated errors in Fig. 7. At 90 and 150 K, the values plotted are those of the original bulk susceptibility, as we assumed the susceptibility does not change at high temperatures. Note that due to the z-axis symmetry for muon at (0,0,0.5), χ_x^{local} must be equal to χ_y^{local}. The solid curves in Fig. 7 are theoretical fits based on a CEF calculation to be detailed in Sec. V. The dashed line representing χ^{bulk} was calculated according to expression (4), using $\lambda=-5.4$ mole/emu, which is close to a previously reported value of -6.23.[4] This dashed line is also plotted as a fit to the data in Fig. 1. The most striking feature of Fig. 7 is the anisotropy of the new local susceptibility. It is easy to understand that the muons' location on one of the principle axes should induce an anisotropy in the original cubic unit cell. This symmetry consideration is the basis for a quantitative analysis of the new susceptibility, which will be described in the next section.

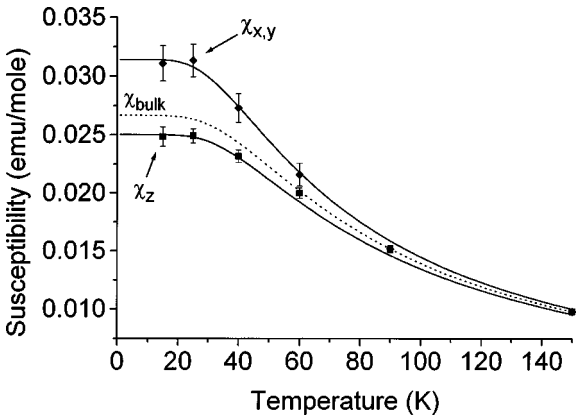

FIG. 7. Modified magnetic susceptibility of the two Pr ions next to the μ^+, along the principle axes. $\chi_{x,y}$ is calculated from $K_{F1}(T)$ and χ_z from $K_{F2}(T)$. The solid lines are a theoretical fit based on a proposed modified CEF for these ions (see Sec. VI). The dashed curve is the original isotropic $PrIn_3$ bulk susceptibility.

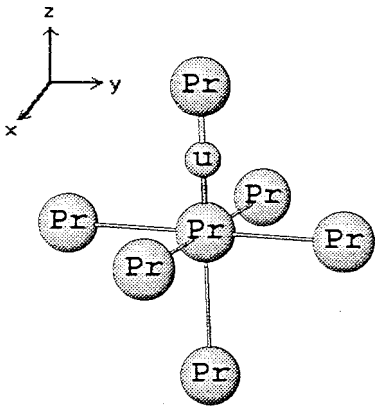

FIG. 8. Muon site relative to neighboring Pr ions. The configuration is identical for both sites.

As a last remark we return to check the assumption we made concerning $\mathbf{A}_{\rm con}$ while calculating $\chi_{\rm local}$ [assumption (iii)]. This assumption must be checked carefully because, although the contact interaction decays with distance, it does so in an oscillatory manner. Hence, in reality, there may be an error in our involving just the two nearest neighbors in the contact interaction. In order to make sure that our calculated $\chi^{\rm local}$ will not be affected greatly by such a misfortune, we carried out a second computation of $\chi^{\rm local}$, analogous to the one described by Eqs. (17) and (18), but this time assuming that the contact field involves all other Pr ions *except* the nearest ones. This means we replaced the elements $A_{\rm con}\chi^{\rm local}$ in Eqs. (17) and (18) by $A_{\rm con}\chi^{\rm bulk}$, with the same value of $A_{\rm con}$. Note that any more realistic mixed contribution from the nearest and the non-nearest ions will fall somewhere in between the results of these two calculations. However, we find that the local susceptibility obtained with the second calculation always fell well within the error boundaries of the first calculation. This means that any error in our third assumption above is of minor importance to the conclusions.

V. THEORETICAL MODEL FOR LOCAL SUSCEPTIBILITY

In accord with expression (3), the observed $\chi_{\rm local}$ is directly related to a change in the local CEF energy levels. In order to fit a theoretical line to $\chi_{\rm local}$ (Fig. 7), we must modify $\mathcal{H}_{\rm CEF}$ so as to obtain the required level changes. However, the changes in $\mathcal{H}_{\rm CEF}$ must also agree with the new charge distribution around the Pr ion. In Fig. 8 we see that the symmetry existing now around each of the neighboring Pr ions is not the original cubic symmetry, but rather the tetragonal C_{4v} symmetry. Note that the symmetry will remain C_{4v} even if we take into account possible muon-induced changes in the charge distribution because these changes must be axially symmetric with respect to the z axis (as long as we allow no spontaneous symmetry breaking in the xy plane). The general Hamiltonian describing C_{4v} symmetry is

$$\mathcal{H}_{\rm CEF,tet}=B_2^0O_2^0+B_4^0O_4^0+B_4^4O_4^4+B_6^0O_6^0+B_6^4O_6^4. \quad (19)$$

Expression (19) has five free parameters, compared to two in the original cubic Hamiltonian (1). In principle, the μ^+ may modify the charge distribution existing around the Pr ions in every direction. However, to simplify matters we will now assume we need considering only changes occurring along the z axis. Our main justification for such an ''axial assumption'' is that the charged muon is itself the dominant disturbance to the original charge density and it is located on the z axis. We may now separate the charge distribution around each neighboring Pr ion into two parts: a cubic distribution *similar* to the original charge distribution and a second distribution containing the effects of the muon. Following our assumption, this second part must have *complete* axial symmetry, meaning that it will be dependent only on z. The above charge distribution separation will naturally divide each of the B_l^m coefficients given by expression (2) into two parts: the original cubic coefficient and an axial addition created by the muon's presence. This we will designate by $B_{l,\rm axial}^m$.

We now show that $B_{4,\rm axial}^4=B_{6,\rm axial}^4=0$. Looking at expression (2) for the B_l^m parameters, we remember that any spherical harmonic of the type Y_l^4 is always dependent on Φ only through the factor $\exp i4\Phi$. If we now add to this our assumption that the charge density $\rho_{\rm axial}$ is independent of Φ, we arrive at the conclusion that

$$B_{l,\rm axial}^4\sim\int_R\int_\Theta\frac{\rho_{\rm axial}(R,\Theta)}{R^{l+1}}\,Y_l^{4*}(\Theta)\int_{\Phi=0}^{2\pi}\exp\,i4\Phi d\Phi=0,$$

which means that B_4^4 and B_6^4 in Eq. (19) will remain at their cubic values, reducing the number of free parameters from five to three. Notice that for the coefficients $B_4^0=B_6^0$ the same reasoning leads to a different result:

$$B_{l,\rm axial}^0\sim\int_R\int_\Theta\frac{\rho_{\rm axial}(R,\Theta)}{R^{l+1}}\,Y_l^{0\star}(\Theta)\int_{\Phi=0}^{2\pi}1d\Phi\neq0.$$

Thus the values of these coefficients remain free.

In order to fit the new susceptibility we may also consider changing the values of the Landé g factor and the exchange coupling parameter λ [see Eq. (4)]. However, because the $4f$ electrons are well screened from their electronic environment, we chose to ignore changes in the g factor.

Our best theoretical fit is shown as solid curves in Fig. 6. The fitted CEF parameters are $B_2^0=0.031$ meV, $B_4^0=-0.0018$ meV, $B_4^4=-0.001\,26$ meV (as in a cubic field), $B_6^0=0.000\,04$ meV, $B_6^4=-0.0013$ meV (as in a cubic field), and $\lambda=-4.8$ mole/emu. Note that the factors of 5 and -21 existing between the cubic parameters in Eq. (1) are not preserved in the new Hamiltonian.

The fitted curves describe the data remarkably well. The anisotropy, which is consistent with the new CEF, diminishes with increasing temperature and the local and bulk susceptibility converge at high temperatures. Remember that one of our basic assumptions in calculating the new susceptibility from the data of Fig. 6 was that the susceptibility remain unchanged at high temperatures. Here we see that changing the CEF is prone to cause significant changes only at lower temperatures. This, then, is the theoretical justification for our treatment of the results in Fig. 6. The fitting procedure was simplified after noting that varying B_2^0 alone introduces immediately a significant anisotropy between the z and x directions, lowering one and raising the other, while

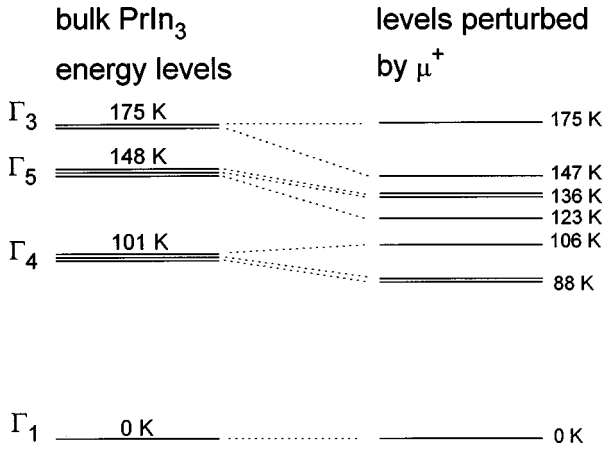

FIG. 9. Original bulk energy-level scheme of $PrIn_3$ (left), compared to the local level scheme induced by the μ^+ (right).

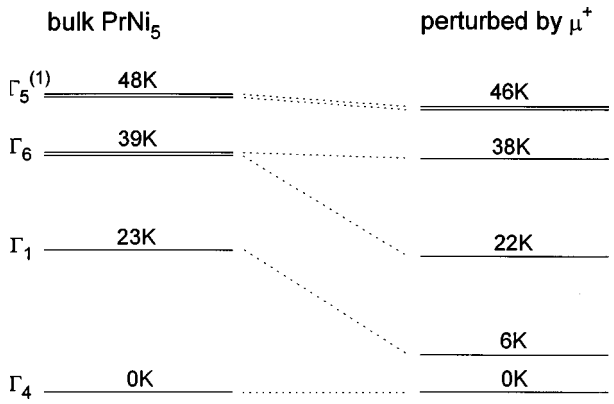

FIG. 10. Original bulk energy level scheme of the Pr ions in $PrNi_5$ (Ref. 12), compared to the local level scheme produced by the μ^+. The figure is taken from Ref. 1.

keeping the symmetry between the x and y directions. Thus first a rough fit was affected by changing the value of B_2^0 and this was then refined by letting the other parameters vary.

We checked also the possibility of freeing B_4^4 and B_6^4, i.e., relaxing the axial assumption. We found, however, that changing these parameters by a few percent causes only minor modifications to the susceptibility. The conclusion is that our assumption is not crucial for obtaining the best-fit CEF, but it also means that the validity of the assumption may not be tested in a critical manner within the experimental accuracy of the data in Fig. 7. Finally, we note that a fit could not be obtained by leaving the cubic CEF unchanged and varying *only* the exchange parameter λ. This is because varying λ always changes the y and z susceptibilities in the same direction, raising or lowering both, in contrast to our results (Fig. 7).

The change in the CEF parameters is of course equivalent to a rearrangement of the local energy levels. The new local level scheme is shown in Fig. 9 (right-hand side). In general, we note that the muon causes a lowering of the energy levels by 10–20 K. The apparent *downward* trend may be expected from the fact that the muon is positively charged and so reduces the potential energy of the electrons in its vicinity.

VI. DISCUSSION

We may now discuss some of the present results for $PrIn_3$ in comparison with the only other system for which μ^+-induced effects are reported, namely, $PrNi_5$.[1] Unlike our present cubic bulk system, $PrNi_5$ is hexagonal, with a well-known large axial anisotropy of the susceptibility.[10,11] Nevertheless, examining Figs. 9 and 10, we note a qualitative similarity of the μ^+ influence on the local energy levels in both systems. In general, both exhibit a *reduction* of the local energy levels. Perhaps even more remarkable is the similar *magnitude* of the energy level changes, around 10–20 K for both systems. A first-principles theory to account for the numerical value (10–20 K) of the observed level reduction is not available at present. However, the similarity of the effects on the electronic levels in both systems is perhaps not surprising, as the main energy term involved in ''implanting'' a positive muon in either system originates from the same Coulomb interaction with the electronic distribution around neighboring atoms.

A quite different situation is encountered when comparing μ^+-induced *magnetic* effects in both systems. In $PrIn_3$ (see Fig. 7), χ_i^{local} deviate from χ_i^{bulk} by 20% at most. In contrast, deviations of up to an order of magnitude are observed in the low-temperature limit for the local susceptibility in $PrNi_5$.[1] This marked difference in the influence of positive muons on local magnetic properties is fully accounted for by the detailed, if not always transparent, analysis presented in previous sections here and in Ref. 1. Some insight to the physical origin of this difference may be obtained by examining again the theoretical expression (3). The ground state of both crystals is a magnetic singlet and therefore the dominant term in the low-temperature susceptibility will be the van Vleck $E_n^{(2)}$ term, with $n=0$ indicating ground level. However this term is *reciprocally* dependent on the height of the next excited levels. Thus changes in $E_0^{(2)}$ will depend on the *relative* shift of the energy levels (relative to the original spacing) rather than on the absolute value of the shift. By comparing Fig. 9 with Fig. 8 it is clear that in $PrNi_5$ the relative shift of the energy levels is much greater and so we would expect a more drastic influence on the susceptibility. In particular, let us look at the first excited level of the two crystals. The first excited level of $PrNi_5$ is at 23 K. This level shifts down by 17 K, to a new value of 6 K. In the low-temperature limit, this lowering should change the susceptibility by a factor of the order of $\frac{1}{6}:\frac{1}{23}\cong 4$. In contrast, the $PrIn_3$ susceptibility is expected to change only by a factor of the order of $\frac{1}{88}:\frac{1}{101}\cong 1.2$. In summary, a similar shift of energy levels in both cases will (and does) produce a very different effect on the low-temperature susceptibility.

VII. CONCLUDING REMARKS

In this paper we have presented experimental μSR results that show that the charged μ^+ has a definite influence on the CEF acting on neighboring Pr ions in $PrIn_3$. In other words, the muon may not be treated in this case as a perfect probe for measuring the true magnetic properties. The perturbation induced by the muon was quantitatively presented as a shift in the CEF energy level scheme. Comparing the energy shifts found in this work with those found earlier in $PrNi_5$,

we conclude that the magnitude of the electronic perturbation is approximately the same. However, the influence of this perturbation on the magnetic properties of the two crystals is quite different. Considering these results, it is obvious that in order to use μSR as a reliable tool for studying magnetic properties, one should have some general rule indicating when the muon is prone to cause a significant perturbation and when it may be safely neglected. As a first step towards that goal, we have planned a complete set of measurements all dealing with van Vleck paramagnets of the type PrX_n. The two crystals discussed, $PrIn_3$ and $PrNi_5$, are the first two of this set. At present μSR data are being gathered on the single-crystal $PrPb_3$ and preliminary results seem consistent with the above. Other candidates are $PrSn_3$ and $PrTl_3$.[2] Our hope is that as more data are gathered, a consistent pattern will emerge, which may provide the basis for a rigorous theoretical calculation able to foresee the extent of the effect in various experimental situations.

ACKNOWLEDGMENTS

We are grateful to A. Furrer for providing the program for CEF calculations, to R. Feyerherm for assistance with the program, and to I. Felner for the susceptibility data. Part of this research was supported by the Israel Science Foundation (Israel Academy of Science).

[1] R. Feyerherm, A. Amato, A. Grayevsky, F. N. Gygax, N. Kaplan, and A. Schenck, Z. Phys. B **99**, 3 (1995).

[2] W. Grob, K. Knorr, A. P. Murani, and K. H. J. Buschow, in *Crystal Field Effects in Metals and Alloys*, edited by A. Furrer (Plenum, New York, 1977), p. 37.

[3] A. Grayevsky, I. Felner, T. Tashma, N. Kaplan, F. Gygax, A. Amato, M. Pinkpank, and A. Schenck, Hyperfine Interact. **104**, 73 (1997).

[4] K. Buschow, H. W. de Wijn, and A. M. van Diepen, J. Chem. Phys. **50**, 137 (1969).

[5] H. L. Schläfer and G. Glielmann, *Basic Principles of Ligand Field Theory* (Wiley-Interscience, New York, 1969).

[6] A. Abragam and B. Bleaney, *Electron Paramagnetic Resonance of Transition Metal Ions* (Clarendon, Oxford, 1970).

[7] J. van Vleck, *Electric and Magnetic Susceptibilities* (Oxford, New York, 1932).

[8] A. Schenck, in *Frontiers in Solid State Science*, edited by L. C. Gupta and M. S. Murani (World Scientific, Singapore, 1993), Vol. 2.

[9] A. Grayevsky, T. Tashma, I. Felner, Z. Kalman, N. Kaplan, F. Gygax, A. Amato, M. Pinkpank, and A. Schenck, Hyperfine Interact. **104**, 67 (1997).

[10] K. Andres, S. Darack, and H. R. Ott, Phys. Rev. **19**, 5475 (1979).

[11] V. M. T. S. Barthem, D. Gignoux, A. Nait-Saada, D. Schmitt, and G. Creuzet, Phys. Rev. B **37**, 1733 (1988).

[12] A. Amato, W. Bührer, A. Grayevsky, F. N. Gygax, A. Furrer, N. Kaplan, and A. Schenck, Solid State Commun. **82**, 767 (1992).

[13] *International Tables for Crystallography*, edited by T. Hahn (Reidel, Dordrecht, 1987), Vol. A, p. 662.